Supplement of The Cryosphere, 12, 3311–3331, 2018
https://doi.org/10.5194/tc-12-3311-2018-supplement

The Cryosphere Open Access EGU

Supplement of

19th century glacier retreat in the Alps preceded the emergence of industrial black carbon deposition on high-alpine glaciers

Michael Sigl et al.

Correspondence to: Michael Sigl (michael.sigl@psi.ch)

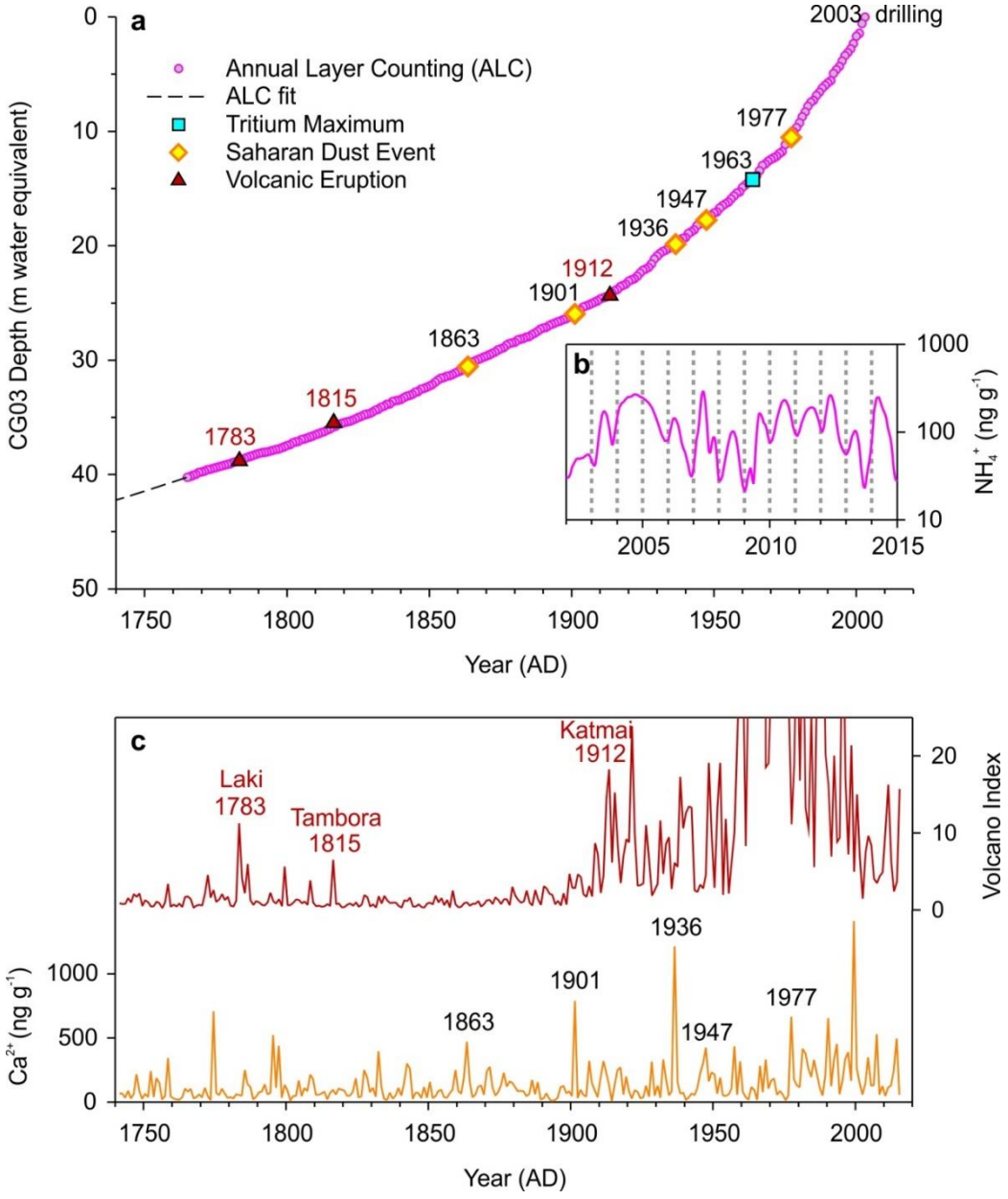

Supplementary Fig. S1: Colle Gnifetti timescale **a)** Depth-age relationship for CG03 based on combining annual-layer counting with distinctive reference horizons (Jenk et al., 2009); **b)** CG15 NH_4^+ concentrations used for extending the chronology into the present. **c)** Volcano Index (defined as Volcano Index = $[SO_4^{2-}]^2/[Ca^{2+}]$) and Ca^{2+} concentrations used to identify volcanic eruptions and historic Saharan dust events (Wagenbach et al., 1996; Oeschger et al., 1977).

Supplementary Table S1: Age markers for the Colle Gnifetti ice cores.

Type of Age Marker	Parameter	Year (AD)	CG03A Depth (m)	CG03B Depth (m)
SDE 1977	Ca^{2+}, Fe	1977	18.90	18.88
NWT	^{3}H	1963	24.45	n.a.
SDE 1947	Ca^{2+}, Fe	1947	29.23	29.32
SDE 1936	Ca^{2+}, Fe	1936	31.96	32.03
Katmai 1912	SO_4^{2-}, SO_4^{2-}/Ca^{2+}	1912	37.31	37.44
SDE 1901	Ca^{2+}, Fe	1901	39.20	39.28
SDE 1863	Ca^{2+}, Fe	1863	44.36	44.46
Tambora 1815	SO_4^{2-}, SO_4^{2-}/Ca^{2+}	1816	49.79	49.79
Laki 1783	SO_4^{2-}, SO_4^{2-}/Ca^{2+}	1783	53.50	53.42
Bedrock		-17000	80.18	81.14

SDE = Historic Saharan Dust Event (Wagenbach et al., 1996; Oeschger et al., 1977); NWT = Maximum of northern hemisphere nuclear weapon testing; n.a. not analyzed

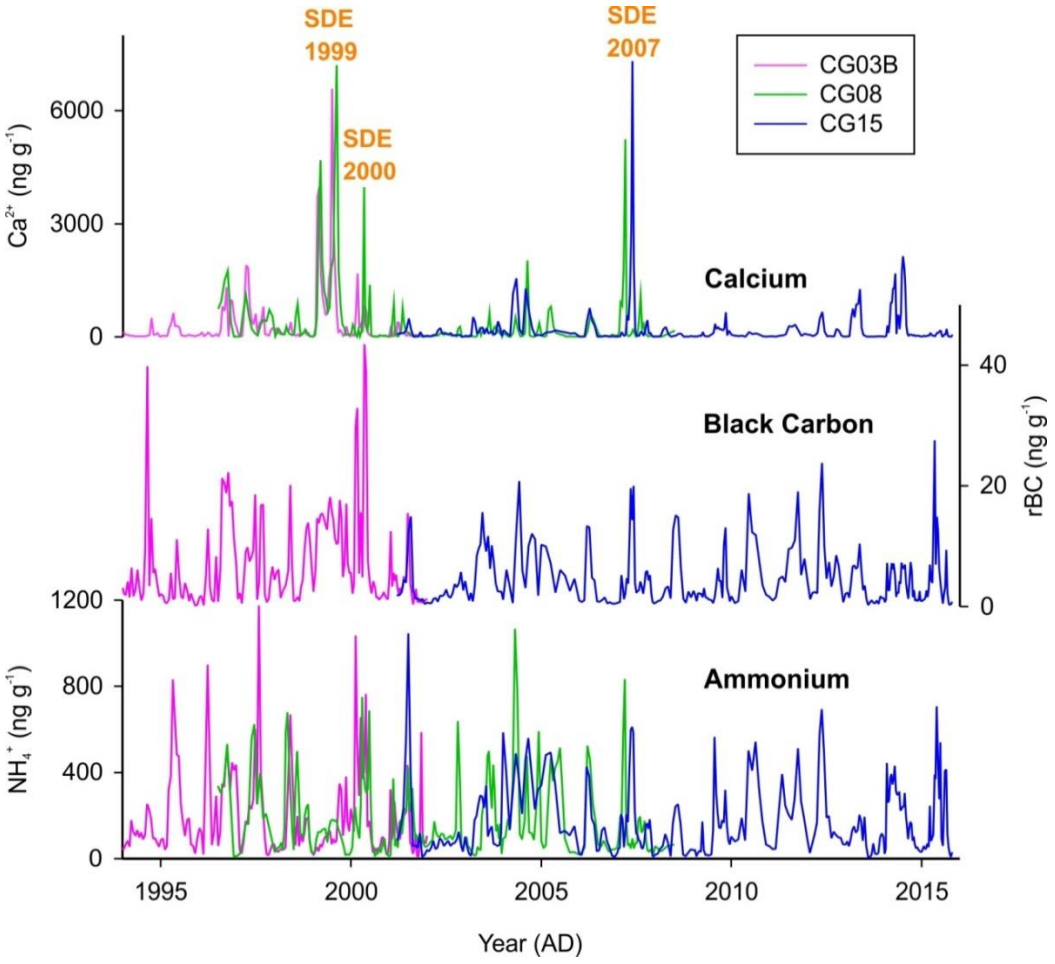

Supplementary Fig. S2: Comparison of selected tracers for the three ice/firn cores CG03B, CG08 and CG15. CG03B was dating by synchronization with CG03A, whereas CG08 and CG15 were dated by counting annual layers.

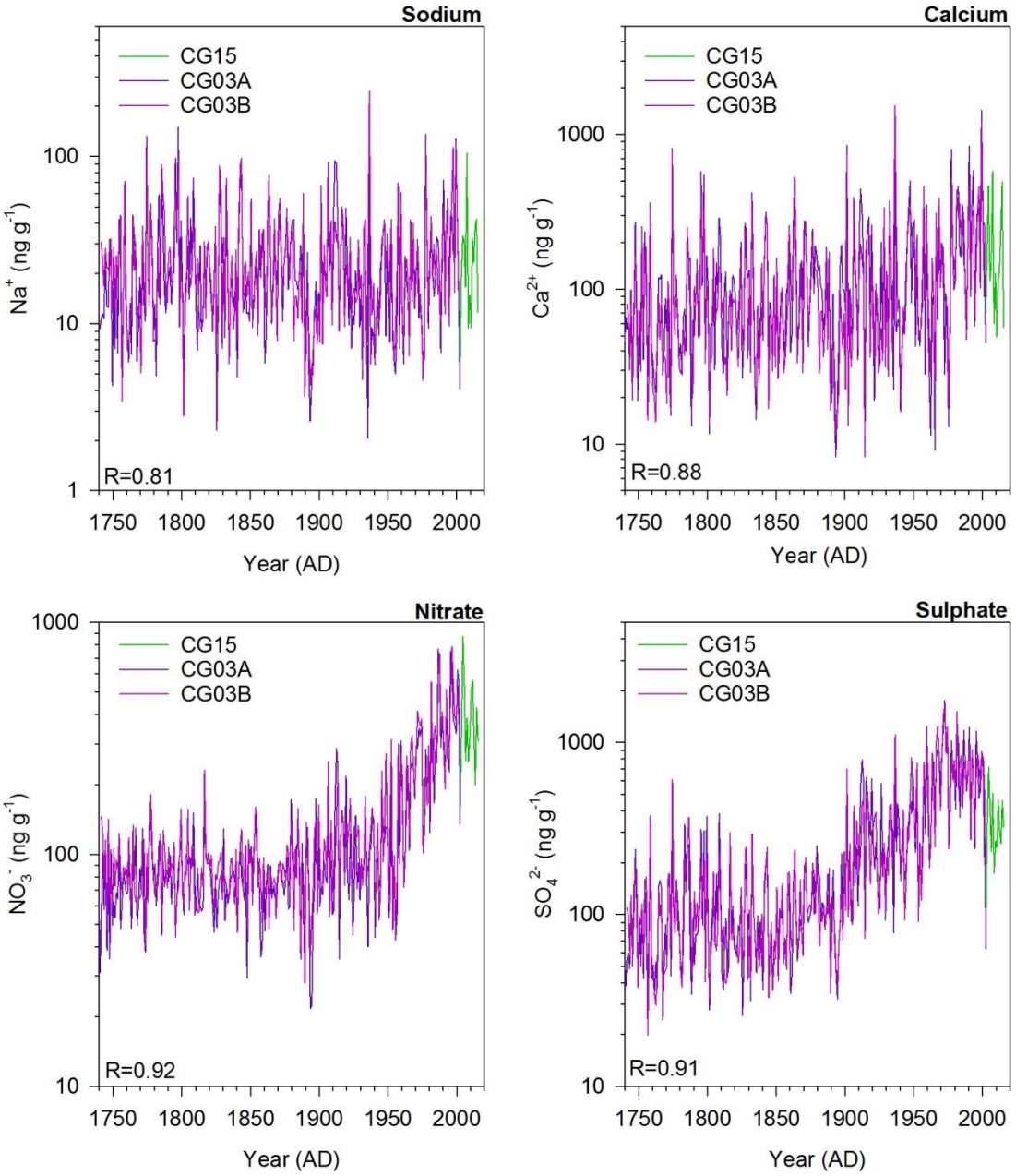

Supplementary Fig. S3: Annual concentrations of selected tracers for the new ice core CG15 and the two parallel cores CG03A and CG03B (1741-2015 AD) with *Pearson's* correlation coefficient (R) indicated.

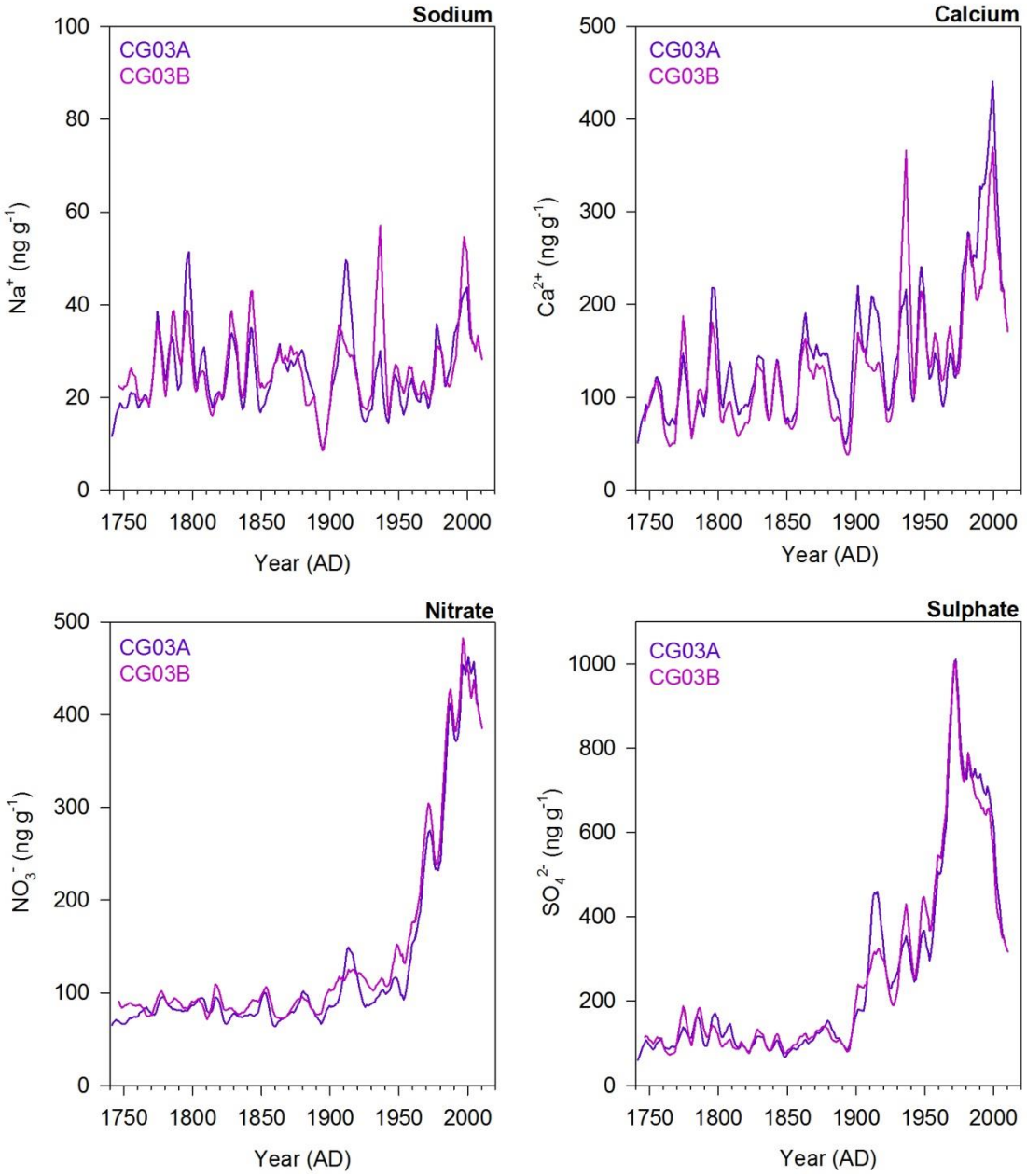

Supplementary Fig. S4: Concentrations of selected tracers for the two parallel cores CG03A and CG03B (1741-2002 AD) extended using CG15 (2003-2014 AD). All records were smoothed with an 11-year filter.

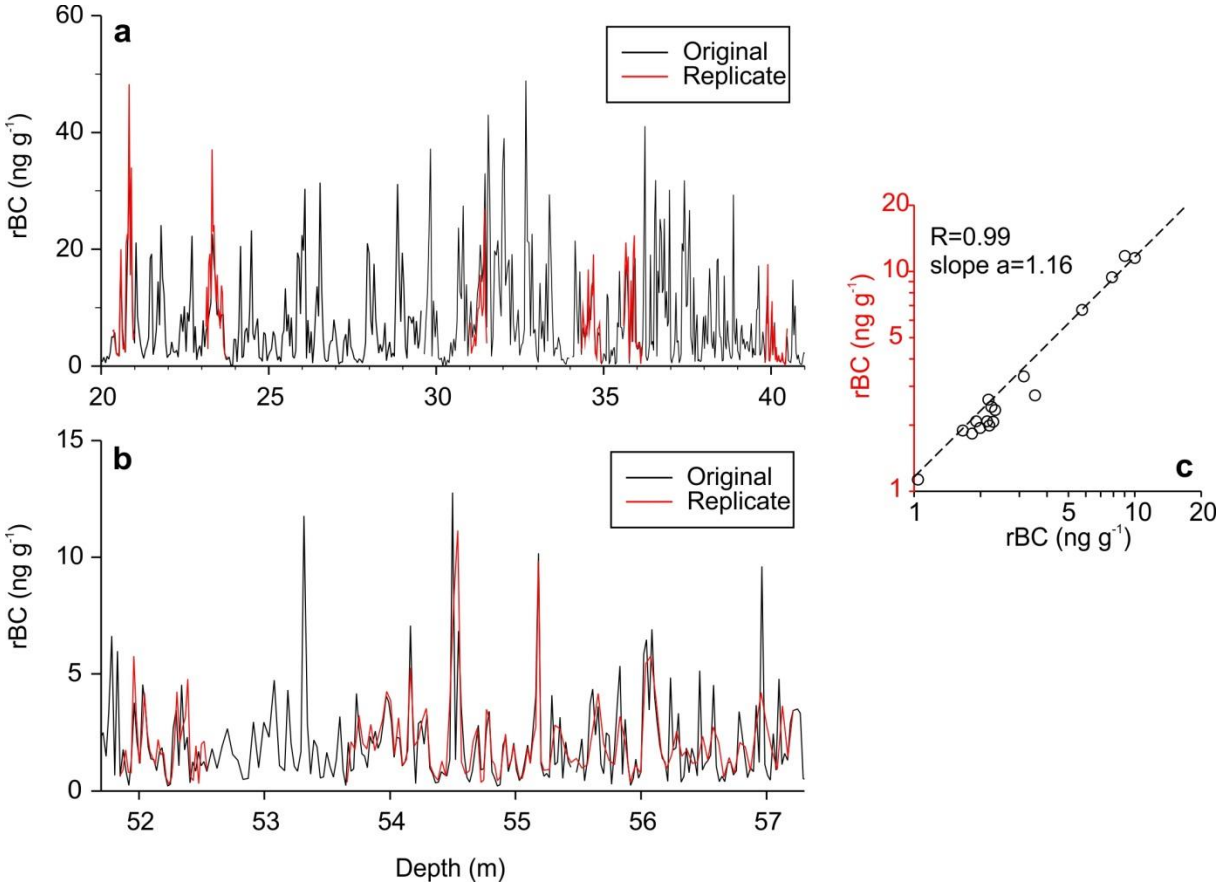

Supplementary Fig. S5: a) Comparison of original analyses and replicate analyses for CG03 **a)** during the industrial period (1888-1975 AD) and **b)** during the preindustrial period (1740-1799 AD). **c)** mean concentrations determined for all ice-core sections with available replication samples with a linear fit against mean values from the original analysis with *Pearson's* correlation coefficient (R) indicated.

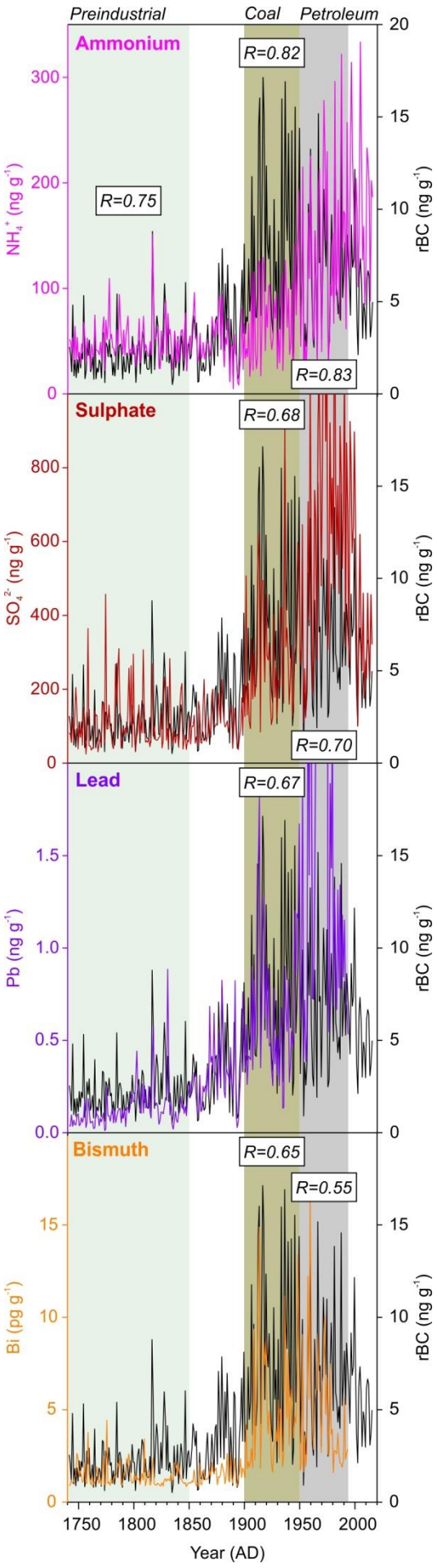

Supplementary Fig. S6: Colle Gnifetti rBC record compared with selected glaciochemical and trace element records. *Pearson's* correlation coefficients (P<0.0001; 1-sided) are displayed for time periods dominated by preindustrial emissions (1741-1850 AD), coal burning (1901-1950 AD) and burning of petroleum products emissions (1951-1993 AD), respectively.

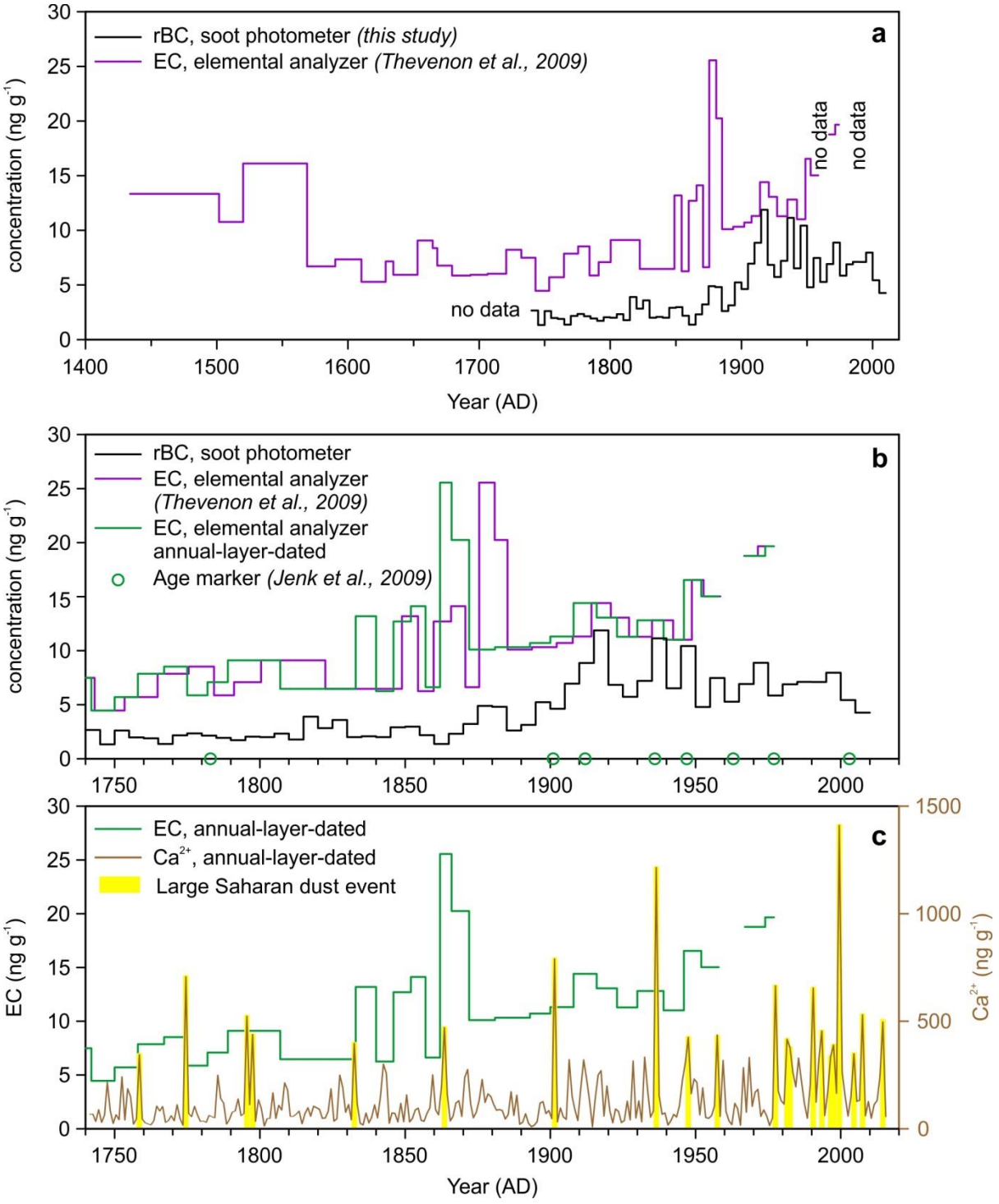

Supplementary Fig. S7: a: Colle Gnifetti 5-year averaged rBC concentrations (black) and Colle Gnifetti elemental carbon (EC, purple) concentrations (Thevenon et al., 2009) resampled to a temporal resolution >4 years. Note that the EC record is shown on a modeled ice-core chronology (Thevenon et al., 2009); **b:** EC record on the modeled chronology (purple) has a mean 19th century age bias of +14 years compared to the annual-layer dated timescale (Jenk et al., 2009; green) constrained by absolute-dated stratigraphic age markers (green circles); **c**: Colle Gnifetti EC concentrations (green) compared with Colle Gnifetti Ca^{2+} concentrations, a tracer for mineral dust, peaking during Saharan dust deposition events (yellow).

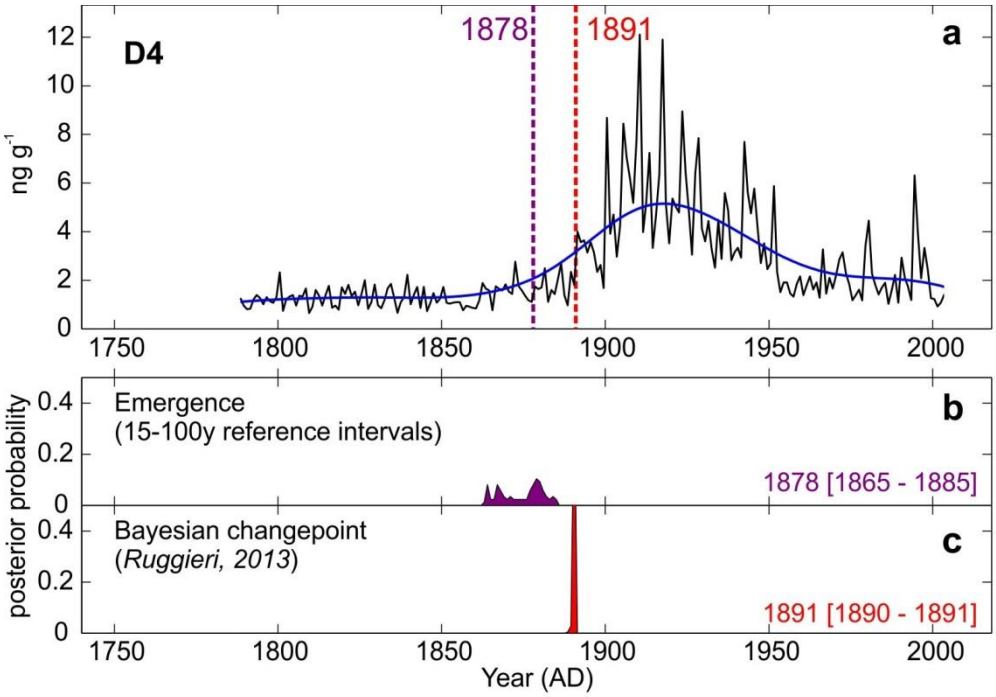

Supplementary Fig. S8: As Fig. 7 but for BC concentrations from the Greenland D4 ice-core corrected using vanillic acid to discriminate BC spikes from forest fires.

5

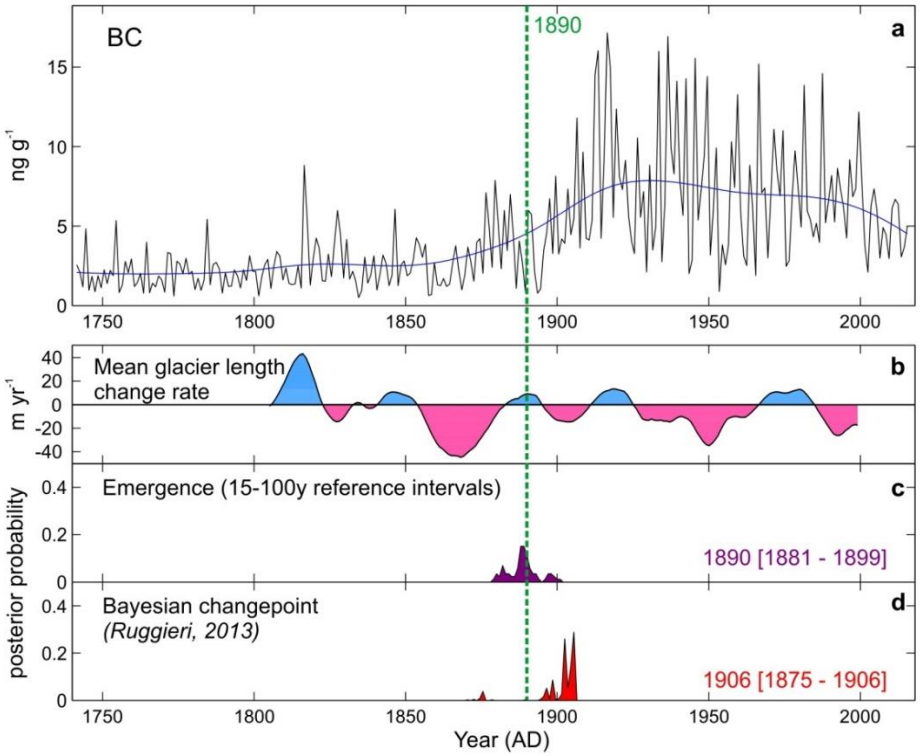

Supplementary Fig. S9: As Fig. 7 but for total BC concentrations

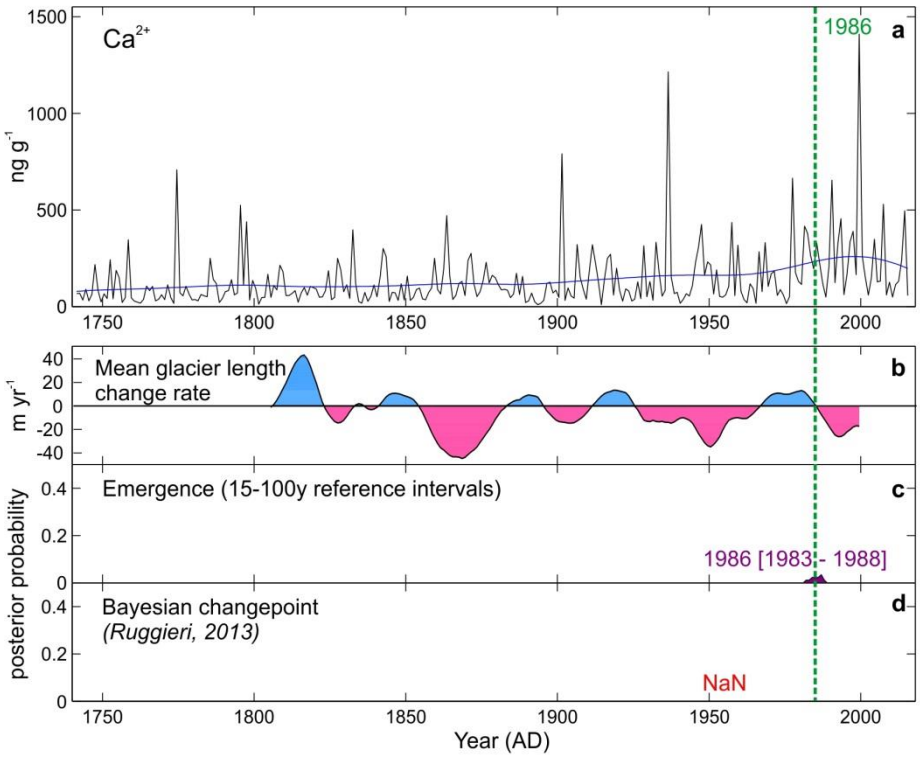

Supplementary Fig. S10: As Fig. 7 but for total Ca^{2+} concentrations

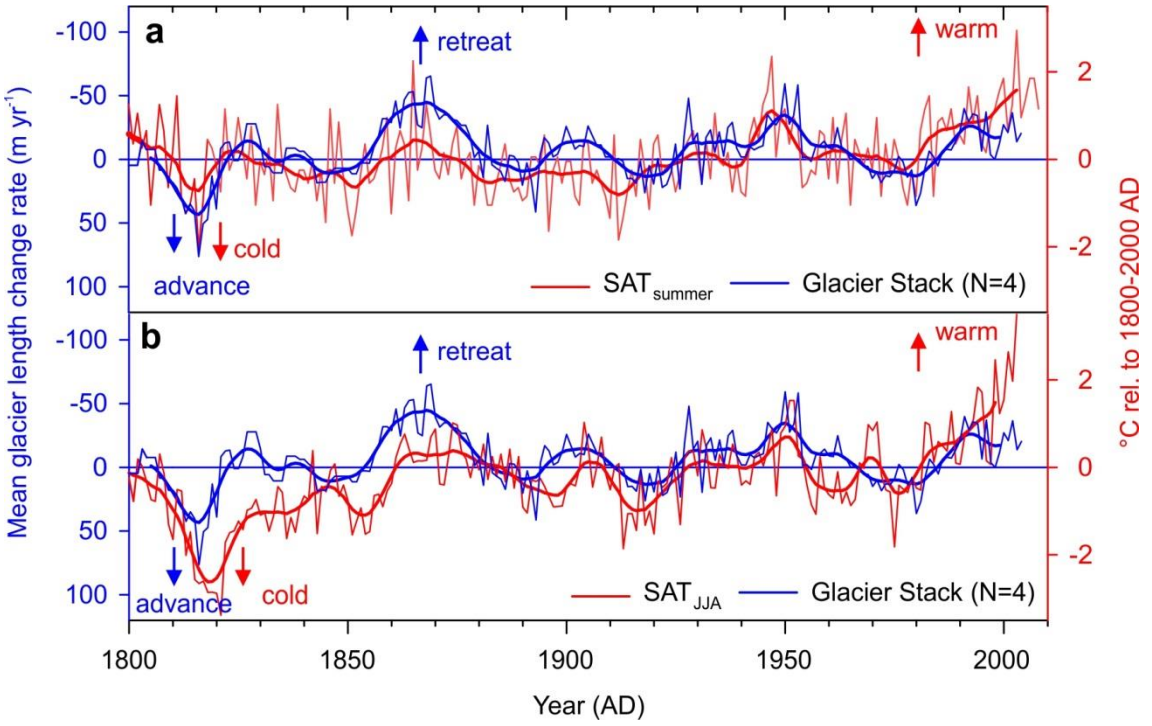

Supplementary Fig. S11: a) Smoothed and annual resolution mean glacier length change rates of the *Glacier Stack* and equally resolved surface air temperature anomalies for the summer half year (SAT_{summer}) from the Greater Alpine Region HISTALP station network (Böhm et al., 2010); note that the curves are displayed inverse compared to Fig. 8; **b)** the same *Glacier Stack* curves compared with a June-August surface air temperature reconstruction for the greater Alpine region based on tree-rings (Büntgen et al., 2011).

Supplementary References:

Büntgen, U., Tegel, W., Nicolussi, K., McCormick, M., Frank, D., Trouet, V., Kaplan, J. O., Herzig, F., Heussner, K. U., Wanner, H., Luterbacher, J., and Esper, J.: 2500 Years of European Climate Variability and Human Susceptibility, Science, 331, 578-582, 2011.